Iraqi Journal of Science, 2024, Vol. 65, No.1, pp: 186- 197
DOI: 10.24996/ijs.2024.65.1.17

ISSN: 0067-2904

The Effect of Doped TiO_2 Layer on the Performance and Stability of PCDTBT: PCBM-based Organic Solar Cells

Mohammed K. Al-hashimi[1], Ameer F. Abdulameer[2]*, Hikmat A. J. Banimuslem[3], Yaqub Rahaq[4]

[1]Department of Physics, College of Education, University of Misan, Misan,, Iraq
[2]Department of Physics, College of Science, University of Baghdad, Baghdad,, Iraq
[3]Department of Physics, College of Education, University of Babylon, Babylon,, Iraq
[4]Material and Engineering Research Institute, Sheffield Hallam University, UK

Received: 5/1/2023 Accepted: 12/7/2023 Published: 30/1/2024

Abstract

Charge extraction layers play a crucial role in developing the performance of the inverted organic solar cells. Using a transparent metal oxide with appropriate work function to the photoactive layer can significantly decrease interface recombination and enhance charge transport mechanism. Therefore, electron selective films that consist of aluminium-doped titanium dioxide (TiO_2:Al) with different concentrations of Al (0.4, 0.8, and 1.2)wt % were prepared using sol-gel technique. The inverted organic solar cells PCPDTBT: PCBM with Al doped TiO2 as electron extraction layer were fabricated. It is well known that Al doping concentration potentially affects the physical characteristics of the TiO_2 by controlling the optical, morphological, and structural properties. The effect of Al incorporation on the optical and morphological properties of the prepared films were analysed using UV-Vis spectroscopy, atomic force microscopy (AFM), X-ray diffraction (XRD), and scanning electron microscopy (SEM). The current–voltage (J-V) curves of the PCPDTBT: PCBM organic solar cells show that the TiO2:Al layer with 0.8% Al wt%, has the highest power conversion efficiency which is 3.02%.

Keywords: Al-doped TiO_2, Organic solar cell, PCPDTBT: PCBM, Sol-gel method.

تأثير طبقة TiO2 المطعمة على اداء واستقرارية الخلايا الشمسية العضوية المعتمدة على PCDTBT: PCBM

محمد كاظم الهاشمي[1]*, أمير فيصل عبد الأمير[2], حكمت عدنان جواد[3]، يعقوب شايع الرهق[4]

[1]قسم, الفيزياء، كلية التربية, جامعة ميسان, ميسان, العراق
[2]قسم, الفيزياء، كلية العلوم, جامعة بغداد, بغداد, العراق
[3]قسم, الفيزياء، كلية التربية, جامعة بابل, بابل, العراق
[4]معهد بحوث المواد والهندسة ، جامعة شيفيلد هالام ، المملكة المتحدة

*Email: ameer.abdulameer@sc.uobaghdad.edu.iq

الخلاصة

تلعب طبقات انتزاع الشحنة دورًا مهمًا في تطوير أداء الخلايا الشمسية العضوية المقلوبة (OSCs). يمكن أن يؤدي استخدام أكسيد معدني شفاف بدالة شغل مناسبة للطبقة النشطة ضوئيًا إلى تقليل إعادة الاتحاد في الحد الفاصل بين طبقين بشكل كبير وتعزيز آلية نقل الشحنة. لذلك ،تم تحضير أغشية انتقائية للإلكترون تتكون من ثاني أكسيد التيتانيوم المطعم بالألمنيوم (TiO2: Al) بتركيزات مميزة من (0,4 Al، 0,8 و 1,2) وزن% باستخدام تقنية المحلول الهلامي. تم تصنيع الخلايا الشمسية العضوية المقلوبة PCPDTBT: PCBM مع TiO2 المطعم Al كطبقة لانتزاع الإلكترون. من المعروف جيدًا أن تركيز تطعيم الالمنيوم يؤثر على الخصائص الفيزيائية لـ TiO2 من خلال التحكم في الخصائص البصرية والسطحية والهيكلية. تأثير التطعيم على الخواص البصرية والسطحية للأغشية المحضرة تم تحليلها باستخدام التحليل الطيفي للأشعة المرئية – فوق البنفسجية ، ومجهر القوة الذرية (AFM) ، حيود الأشعة السينية (XRD) والمجهر الإلكتروني الماسح (SEM). تُظهر منحنيات التيار والجهد (JV) للخلايا الشمسية العضوية PCPDTBT: PCBM أن طبقة TiO2:Al بتركيز 0,8٪ من الالمنيوم تمتلك أعلى كفاءة تحويل وهي 3.02٪.

1. Introduction

Recently, there has been widespread utilization of Inverted Organic Solar Cells (IOSCs) to improve the efficiency of Organic Solar Cells (OSCs). This improvement is achieved by employing an electrode with a higher work function and enhanced air stability. To obtain bulk-heterojunction (BHJ) solar cells with effective inversion, interfacial materials of high transparency and conductivity are required, which are added to create a link between the conductive electrode and the photoactive layer. The sol-gel technique was used to produce thin layers (10-40) nm of TiO_2 [1, 2] or ZnO [3–5], which are used as the interfacial layer in Organic Solar Cells (OSCs) and Inverted Organic Solar Cells (IOSCs) [6]. The layers commonly used in organic solar cells (OSCs) exhibit a high degree of transparency in the visible spectrum. The active photoactive layer is covered with a metal oxide layer to prevent oxidation resulting from the high absorption properties in the UV spectrum. This has been found to increase the power conversion efficiency by nearly 80% compared to devices based on PEDOT:PSS of 2.3% efficiency [7,8]. TiO_2 layer, due to its deep valance band maximum and low conduction band minimum compared to the PEDOT:PSS, is being used in the inverted OSCs structure to enhance the electron extraction and hole blocking [9]. Additionally, TiO_2 serves as an electron acceptor layer that facilitates the transfer of charge between the active layer consisting of Poly[9-(1-octylnonyl)-9H-carbazole-2,7-diyl]-2,5-thiophenediyl-2,1,3-benzothiadiazole-4,7-diyl-2,5-thiophenediyl (PCDTBT) and the TiO_2 layer. Including this layer has been found to significantly improve the efficiency of OSCs, ranging from 2.42% to 3.16% [3,10]. It has also been demonstrated in various studies that TiO_2 and its nano-structured layer have an impact on the carrier extraction of the charge and exciton dissociation [11]. Doping TiO_2 with metal ions was reported to improve conductivity, which can be controlled by the quantity of the metal ions [12, 13]. TiO_2 is doped with Al, using $AlCl_3$ and $Al(NO_3)$ as Al-dopant ion precursors [14], using the sol-gel preparation technique This technique is used extensively due to its ease of use, potential to obtain a greater fabrication area, and its low cost compared to other approaches.

The presence of Al as a doping element in a thin film structure could bring the Density Of State (DOS) close to the Fermi energy level and thus improve the density of charge carriers. Due to this, the electrical conductivity may rise [13, 14]. When Al-doped TiO_2 thin film is used instead of the un-doped TiO_2 layer in solar cells, their impedance may decrease, which improves their quality. However, the thickness of the Al-doped TiO_2 layer does not have any impact on the performance of solar cells. Compared to the organic layer, the carrier mobility and concentration of charge carriers of this layer are higher [15]. The author, however, asserts that

the research evaluating the impact of the Al-doped TiO_2 layer on the properties of OSCs is still in its initial stages, and very few outcomes have been attained in this regard.

The present study examines the morphological, structural, and optical features of Al-doped TiO_2 layers with different Al concentrations. The study also examined the impact of these changes on the OSCs' properties as an active layer constructed on hetero-junction. PCPDTBT:PCBM. Current density-voltage (J-V) curves for the different Al doping concentrations were used to analyse the characteristics of these fabricated devices.

2 Materials and Methods

2.1 Materials

The materials employed in this study were obtained from Sigma-Aldrich. These included titanium isopropoxide (TIP) (purity: 97%), [6,6]-phenylC61-butyric acid metheyester (PCBM), Au with a purity of 99.99%, Poly[9-(1- octylnonyl)-9H-carbazole-2,7-diyl]-2,5-thiophenediyl-2,1,3-benzothiadiazole- 4,7-diyl-2,5- thiophenediyl (PCDTBT), Chlorobenzene and Powder sample of Vanadium Oxide V_2O_5.

2.2 Organic Solar Cell Preparation

Processed solution and spin coating process by deposition on glass substrates Indium tin oxide (ITO) were used to create the Organic Solar Cells (OSCs). The glass substrates were pre-structured (with a resistivity sheet of 12Ω/sq) and cleaned by ultrasonic in an alcoholic solution of isopropyl, acetone, and deionized water for ten minutes. The structure of the fabricated OSC is shown in Figure 1. There are four layers in each OSC device: TiO_2 (the electron extraction layer), PCDTBT: PCBM blend (the active layer), V_2O_5 (the hole transporting layer), and Au (the top contact layer).

TiO_2 films were deposited on ITO/glass substrate using the sol-gel technique. TiO_2 precursor solution was prepared in the following procedure: methanol and isopropanol were mixed to create the solvents; titanium isopropoxide (TIP) (titanium precursor) was then added to the solvent's solution at a temperature of 80° C while being continuously stirred. The mixture was later stirred while the acetic acid was carefully added. Figure 2 shows the fabrication processes of the TiO_2 layers. Spin coating of the thin films of TiO_2 was carried out using 2000 rpm spinning speed for 30 seconds, after which it was annealed at a temperature of 600° C. The ellipsometry technique was used to measure the thickness of the TiO_2 thin film created, which was found to be 40 nm.

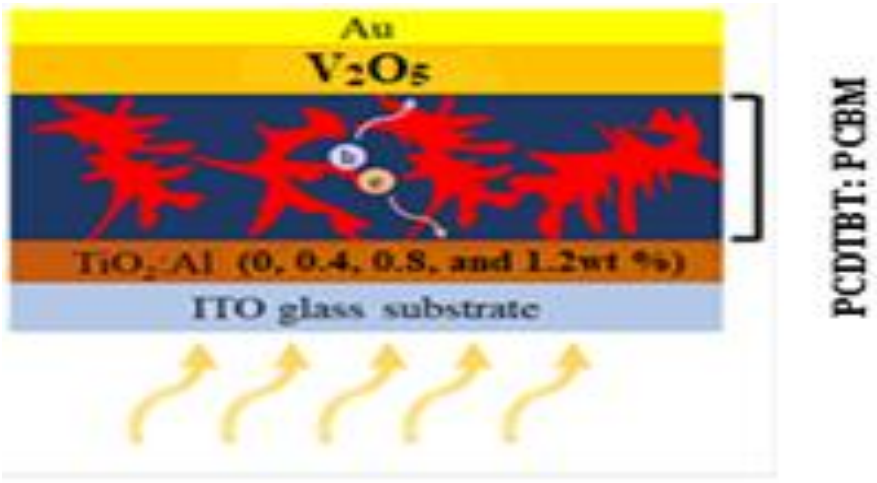

Figure 1: Structure of Fabricated Organic Solar Cell

A solution of PCDTBT and PCBM in chlorobenzene, with a 1:1 ratio, was prepared forthe blend active layer of PCDTBT: PCBM [16]. This layer was deposited over the TiO_2 layer using the spin coating process. The annealing process was subsequently carried out at 120^o C on a hot plate in a glove box in a nitrogen atmosphere for ten minutes [17]. Spin coating of the hole transporting layer of V_2O_5 was carried out over PCDTBT: PCBM active layer, after which it was thermally treated for ten minutes at 110^o C in a nitrogen atmosphere within the glove box. Lastly, 10-6 mbar of vacuum was applied to thermally evaporate 100 nm thickness of a gold (Au) top contact layer, with a deposition rate of 0.1-0.2 nm/sec being used.

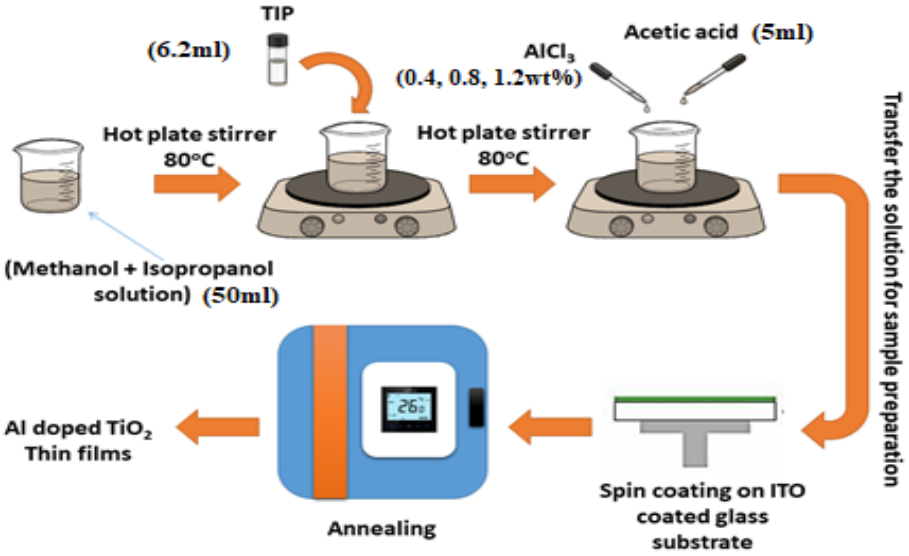

Figure 2: Steps of preparing TiO_2 thin films

3. Characterizations

Scanning electron microscope (FEI-Nova SEM), X'Pert Philips X-ray diffractometer (MPD), and nanoscope multimode AFM (Bruker-AFM) were used to evaluate the structure and morphology of all thin films of Al-doped TiO_2. UV-Visible spectroscopy optically characterized these thin films for wavelengths between 190 and 1100 nm. M200 spectroscopic ellipsometer from the J.A. Woollam Company was used to measure the thickness of the thin film for wavelengths between 370 and 1000 nm. The External Quantum Efficiency (EQE) spectra were measured under the short-circuit condition, i.e. no external current, using an electrometer (Keithley 617S) and xenon lamp as a light source. The light was passed through a monochromator to tune the wavelength of the incident light. The EQE was estimated using the relation EQE (%) = Isc ×124,000 / (λ (nm) ×Pin), where Isc is the short circuit current, λ and Pin are the wavelength and the intensity of incident light, respectively. The 4200 Keithley semiconductor characterization system was used to electrically test the solar cells (i.e., the photovoltaic properties). An intensity of 100mW/cm^2 was generated using AM 1.5 irradiation of the solar simulator.

4. Results and Discussions

The AFM and SEM 3D, and 2D-imaging systems were used to examine Al-doped TiO_2 morphology. The SEM and AFM images of undoped and doped TiO_2 with different concentrations of Al are presented in Figures 3 and 4. The Al concentration was found to have an impact on the surface morphology of TiO_2 films. A decrease in the grain size was noticed with the increase of Al concentration, which may be due to the rise in the number of bulges. In addition, the grain size of TiO_2 decreased when the grain packing density in TiO_2 was increased

by increasing the Al concentration [20, 21]. A flatter surface with fewer bulge structures can be observed in the surface morphology of the 0.8 wt. % Al-doped TiO_2 thin film. The microstructure form of Al-doped TiO_2 can be seen in the film surface images provided by SEM, which comprises various crystalline particles of spherical shapes; particles that do not have a spherical shape can also be seen. The substrate surface is evenly covered by the granules. Hence, the grain structure of TiO_2 particles was altered by Al doping. The microstructure was consistent with compact interconnected grains. In addition, in comparison to pure TiO_2 film, less porosity is exhibited by the doped TiO_2 film, which demonstrates that Al doping may cause the film to become denser [22]. It is clear from the SEM micrographs that when Al doping increased, there was a decrease in the average grain size of TiO_2 [23].

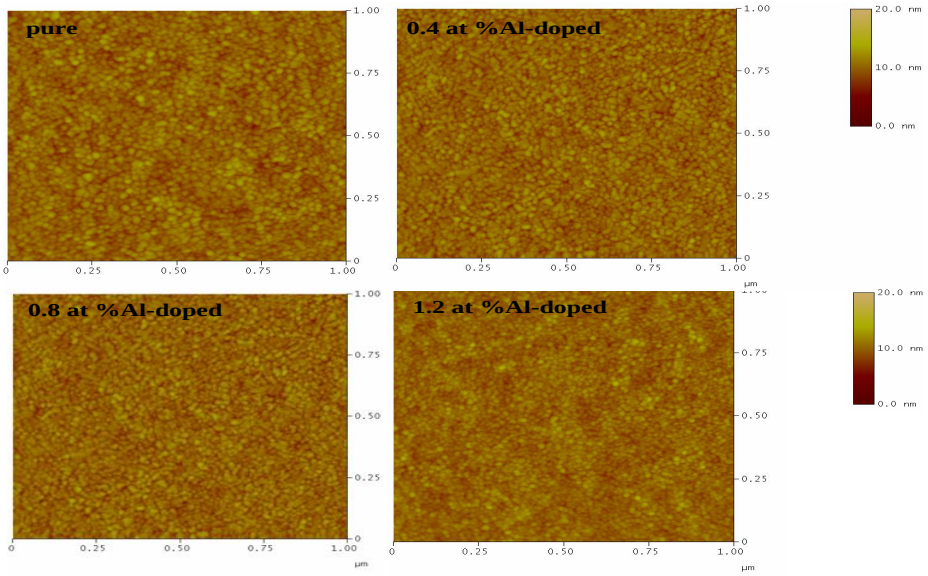

Figure 3: AFM micrographs of Al-doped TiO_2 films with different Al concentrations.

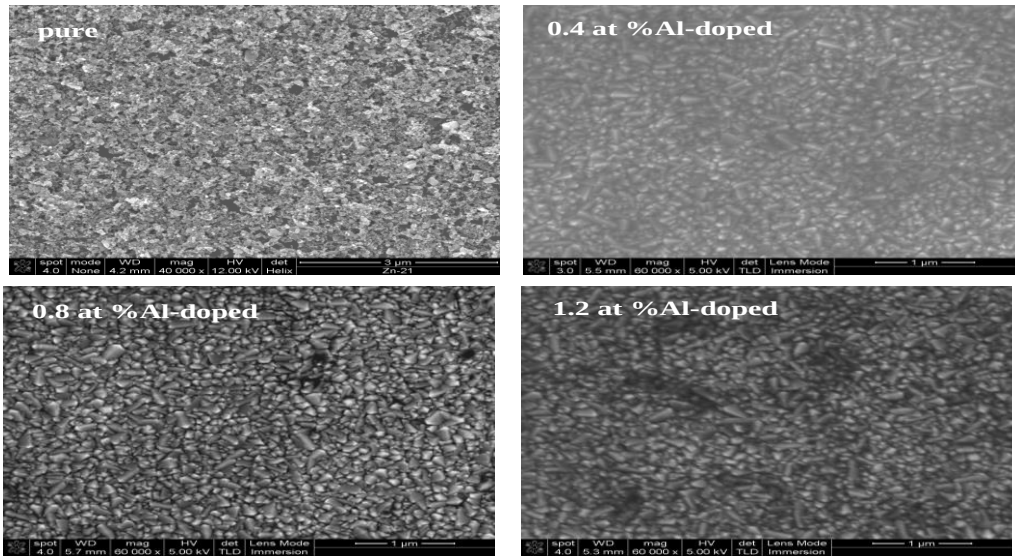

Figure 4: SEM micrographs of Al-doped TiO_2 films with different Al concentrations.

The X-ray diffraction patterns of all created thin films can be seen in Figure 5. The samples are polycrystalline and have preferential axis orientations of (100), (002), (101), (102) and (110). The recorded series, shown in Table 1, exhibited peaks that were identified as originating from the rutile TiO_2 phase. As the Al concentration was increased, a decrease in peaks intensity

and an increase in peaks broadening (FWHM) were noticed. This means that the crystallization of the thin films has decreased, and the rapid diffusion of the Ti interstitials caused a growth in the TiO_2 grains [24].

Using trivalent cation (Al) for doping causes the Ti interstitial content to decrease to balance the loss of charge, and this prevents the TiO_2 grains from growing and hence decreases crystallization [25]. The AFM micrographs show a significant variation between the crystallite size and the grain size; the grain size was significantly bigger than that of the crystalline. The increase in Al content caused a decrease in grain size and minor changes in crystallite size. There is a functional impact of TiO_2 doping on the increase in grain size instead of the crystalline size. These tendencies are found to be associated with the Al-doped TiO_2 inhibition caused by the $AlCl_3$ [26].

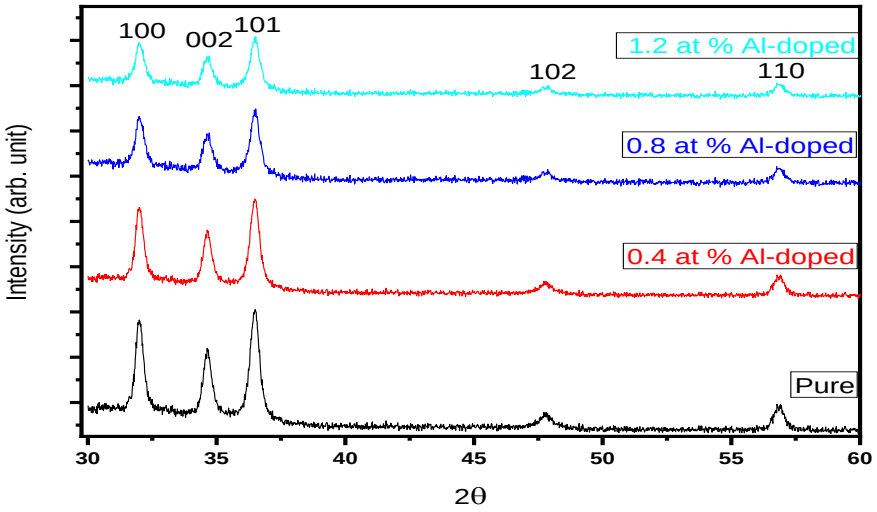

Figure 5: XRD Patterns of TiO_2 thin films doped with different Al concentrations.

Table 1: XRD data for the TiO_2 by using different doping films.

Different doping	Mille Indices (hkl)	Angle (2θ) degree		d values (A)		FWHM Degree	D_{hkl} Nm
		Observed	Stander	Observed	Stander		
0.0	100	31.9405	30.534	2.8082	2.6452	0.2088	41.3524
	002	34.6317	34.321	2.5974	2.3707	0.2134	38.9201
	101	36.5101	36.132	2.4600	2.3130	0.2012	43.4570
0.4%	100	31.9803	31.724	2.7961	2.6462	0.2174	40.2187
	002	34.9720	35.104	2.5984	2.3717	0.2264	38.4570
	101	36.5102	36.151	2.4531	2.3140	0.2152	42.0779
0.8%	100	32.0023	32.124	2.7980	2.6462	0.2223	39.3322
	002	34.9720	34.414	2.5944	2.3717	0.2289	38.0378
	101	36.5110	36.951	2.4421	2.3140	0.2093	41.2536
1.2%	100	32.3103	32.024	2.7861	2.6462	0.2373	36.4230
	002	34.9760	35.140	2.5834	2.3717	0.2668	32.6344
	101	36.6502	36.405	2.4401	2.3140	0.2245	37.2850

Figure 6 shows the differences in the optical properties of un-doped and Al-doped TiO_2 of different concentrations of Al (0.4, 0.8, and 1.2wt %). High transparent spectra are demonstrated by all Al-doped TiO_2 films in the visible range (i.e., 81 to 94%) compared to the un-doped TiO_2 films. This is because of the absorption transitional nature of the Al-doped films. For every sample, there was a sharp transition in the absorption spectrum at a wavelength of around 400 nm [27].

The absorption coefficients (α) were calculated for the samples based on optical transmittance measurements, employing the equation [28]:

$$\alpha = \frac{2.303}{d} \times \log(\frac{1}{T}) \quad (1)$$

Here, d signifies the thickness of the TiO_2 films, whereas T is representative of the transmittance value. Another technique to identify the absorption coefficient of the created thin films is using Equation 2, where the energy of the incident photon needs to be known:

$$\alpha h\upsilon = A\left(h\upsilon - E_g\right)^n \quad (2)$$

Where: h refers to Plank's constant, υ indicates the frequency, A refers to a constant, and n is based on the transition nature. TiO_2 rutile phase is typically related to the direct transport of the semiconductor band gap [29]. Therefore, the direct bandgap of TiO_2 can be determined by examining the $(\alpha h\upsilon)^2$ vs hυ curve through direct transition and extrapolation of the linear region at α = 0, which corresponds to the transition bandgap of n=1/2 [28]. however, the bandgap transition of n=3/2 cannot happen. The relationship between $(\alpha h\upsilon)^2$ and hv of every Al-doped TiO2 film is shown in Figure 6. The linear dependence of $(\alpha h\upsilon)^2$ on hv at high photon energies shows that the Al-doped TiO_2 films are essentially semiconductors with a direct transition. The straight curve part extrapolation to the zero value gives the optical band gap (Eopt). The Eopt values of Al-doped TiO_2 films of (0, 0.4, 0.8, and 1.2 wt.%) Al concentrations are 3.32eV, 3.34eV, 3.36eV, and 3.48Ev, respectively. The Moss-Burstein shift theorem can be used to explain the band gap broadening because the donor electrons can be seen at the conduction band bottom [30]. The Pauli rule does not allow states to be doubly occupied. As the optical transition is vertical, extra energy is required by each valence electron in the higher levels within the conducting bands. As a result, the Al-doped TiO_2 films exhibit broader Eopt compared to the un-doped TiO_2 thin films [30, 31].

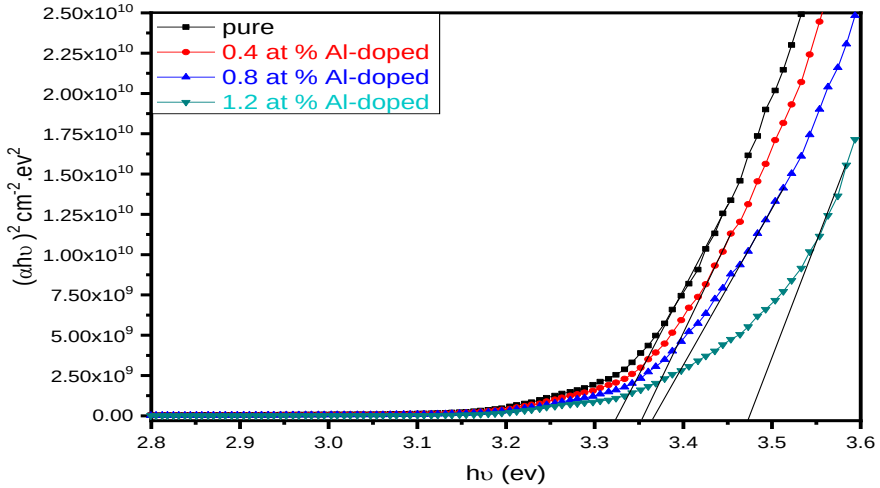

Figure 6 : $(\alpha h\upsilon)^2$ vs. hυ plots of Al-doped TiO_2 films with different Al concentrations

The solar cell spectra of Al-doped TiO_2 with different concentrations of Al are depicted in Figure 7. The figure illustrates that Dye-Sensitized Solar Cell (DSSCs) utilizing Al-doped TiO_2 electrodes exhibit a notable enhancement in incident photon to current efficiency when compared to the un-doped thin film. This increase in efficiency may be attributed to the improved effectiveness resulting from the addition of an electron and charge transfer, along with a greater amount of dye absorption, as indicated in Table 2 [32].

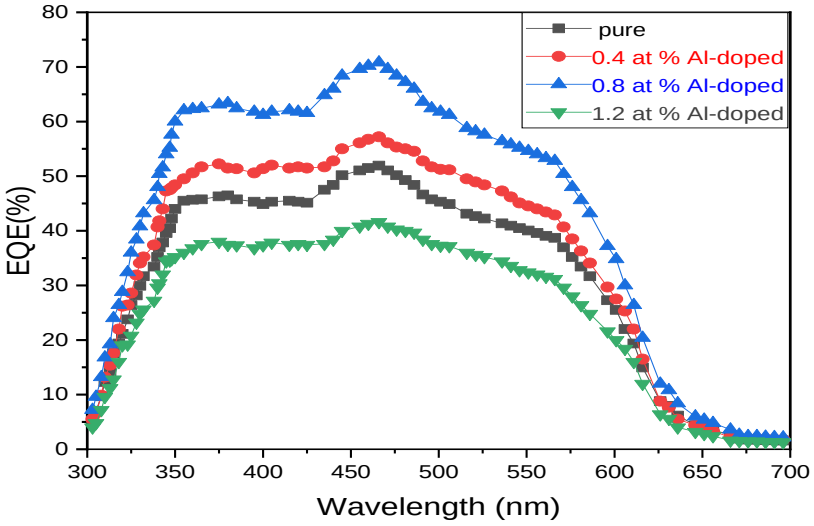

Figure 7 : Effect of different concentrations of Al-doped TiO_2 films on solar cells' spectra

Organic solar cells were created using TiO_2 layers injected with different Al concentrations, after which they were developed using ITO/TiO_2: Al/ PCDTBT: PCBM/ V_2O_5/Au configuration, as depicted earlier in Figure 1. The J-V curves, shown in Figure 8, were used to examine the electrical properties of the manufactured devices. For every manufactured organic solar cell of different Al dopant concentrations, the measurements of J-V curve properties were obtained under illumination with a light source.

The results showed that all the manufactured solar cells displayed a minor increase in short circuit photocurrent density, Jsc ~ 6.65–10.55 mA/cm^2. In addition, a significant change was seen in the open circuit voltage indicator with changes in the Al concentration; the highest of 0.61 V was attained for the 0.8wt% Al-doped TiO_2 layer. The initial variation in the open circuit voltage could be because of the changes in inherent voltage when the Fermi energy level shifted for the donor and acceptor of the Al-doped TiO_2 layer of different Al concentrations (0, 0.4, 0.8, and 1.2 wt. %). There will be an increase in the Fermi energy level toward the conduction band of TiO_2 through Al doping, which occurred due to the shift impact of Burstein–Moss [13, 33-34]. Nevertheless, when Al doping concentration was increased further, a higher charge carrier density was obtained. This may explain why the open circuit voltage increases with an increase in Al doping concentration. Table 2 shows the solar cell parameters, density of the short circuit current (Jsc), open-circuit voltage (V_{oc}), fill factor (FF), and power conversion equipment (PCE). Equations 3 and 4 were used to evaluate these parameters [18]:

$$PCE = \left(\frac{J_{max}V_{max}}{P_{max}}\right) \quad (3)$$

$$FF = \frac{J_{max}\, V_{max}}{J_{sc}\, V_{oc}} \quad (4)$$

Where: J_{sc} refers to the short circuit current density ($mA.cm^{-2}$), V_{oc} signifies the open-circuit voltage (V), P_{in} indicates the incident light power, and J_{max} ($mA.cm^{-2}$) and V_{max} (V) refer to the current density and voltage at the point of highest power output in the J-V curves, respectively [19]. There was a slight change in the FF values with changes in Al concentration. Variations in J-V features may occur due to this behavior, which may happen due to the variations in the series resistance. It may also be explained by the modifications in the junction features of the TiO_2/active layer that is also consistent with the energy level and band bending at the junction. Figure 8 shows that the biggest area under the J-V curve is that of the 0.8 wt. % Al-doped TiO_2 J-V curve of the solar cell. This extended area causes the greatest charge carrier extraction [34-36]. For the device with TiO_2 thin film doped with 0.8 wt. % Al, a maximum PCE of 3.02% is obtained.

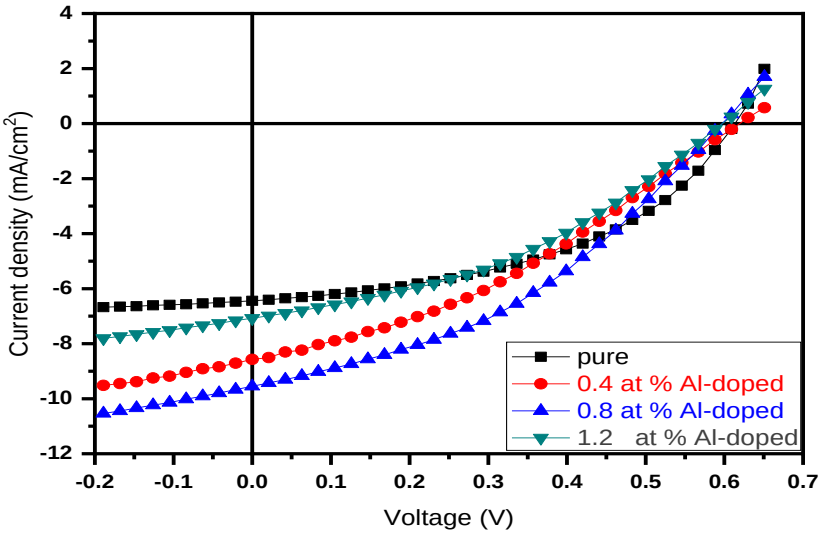

Figure 8 : J–V characteristics of OSCs with undoped and doped TiO_2 layers as function of different Al doping amounts

Table 2: Parameters of OSCs Performance Evaluated via J-V Measurements

Al - content (Wt. %)	Voltage (V_{oc}) (volt)	Current Density (J_{sc}) (mA/cm^2)	Fill Factor (FF) %	Power Conversion Equipment (PCE) %
0.0	0.62 □ 0.01	6.65 □0.2	35 □2	1.44
0.4	0.64 □ 0.02	9.48 □0.4	42 □3	2.5
0.8	0.63 □0.02	10.55 □0.5	47 □3	3.12
1.2	0.64 □0.01	7.85 □0.5	31 □2	1.55

5. Conclusions

The sol-gel process was used to create undoped and doped TiO_2 thin films with different concentrations of Al (0.4, 0.8, and 1.2 wt. %). SEM, UV-Visible, AFM, and XRD measurements were used to examine these thin films. It was concluded from the findings that the grain growth is affected by the doping of the TiO_2 layer with varying Al content, and this may give rise to varying surface morphology. In addition, when Al concentration was increased, the band gap of the fabricated thin films increased, which may be ascribed to the Moss-Burstein

shift. PCDTBT: PCBM polymer blend and Al-doped TiO_2 layer as their transport layer was used to create the inverted type of organic solar cells. The J-V curve was examined as a function of Al doping concentration to review the OSCs. There was an increase in the performance of J-V curves with doped TiO_2 films compared to the undoped film, where the J-V properties of the solar cells with 0.8 wt. % Al was the best. The Al-doped TiO_2 layer affects the parameters of solar cells. There was a significant relationship between the open voltage and the Al doping concentration for the TiO_2 layer, which may be assigned to the shift in the Fermi energy to a higher level in the Al-doped TiO_2 layer. The solar cell properties obtained were significantly related to the properties of the Al-doped TiO_2 layer. It is confirmed that doping the TiO_2 layer with Al influenced the solar cell properties.

References

[1] J. Y. Kim, S. H. Kim, H. H. Lee, K. Lee, W. Ma, X. Gong, and A. J. Heeger, "New Architecture for High-Efficiency Polymer Photovoltaic Cells Using Solution-Based Titanium Oxide as an Optical Spacer," *Adv. Mater*., vol. 18, no. 18, pp. 572-576, 2006.

[2] M. H. Park, J. H. Li, A. Kumar, G. Li, and Y. Yang, "Doping of the Metal Oxide Nanostructure and its Influence in Organic Electronics," *Adv. Funct. Mater*., vol. 19, no. 8, pp. 1241-1246, 2009.

[3] H.-L. Yip, S. K. Hau, N. S. Baek, and A. K. Y. Jen, "Polymer Solar Cells That Use Self-Assembled-Monolayer-Modified ZnO/Metals as Cathodes," *Adv. Mater*., vol. 20, no. 12, pp. 2376-2382, 2008.

[4] M. S. White, D. C. Olson, S. E. Shaheen, N. Kopidakis, and D. S. Ginley, "Inverted bulk-heterojunction organic photovoltaic device using a solution-derived ZnO underlayer," *Appl. Phys. Lett*., vol. 89, no. 14, pp. 143517-143517, 2006.

[5] A. K. K. Kyaw, X. W. Sun, C. Y. Jiang, G. Q. Lo, D. W. Zhao, and D. L. Kwong, "An inverted organic solar cell employing a sol-gel derived ZnO electron selective layer and thermal evaporated MoO3 hole selective layer," *Appl. Phys. Lett.*, vol. 93, no. 22, pp. 221107-221107, 2008.

[6] K. Lee, J. Y. Kim, H. Park, S. H. Kim, S. Cho, and A. J. Heeger, "Air-Stable Polymer Electronic Devices," *Adv. Mater*., vol. 19, no. 18, pp. 2445-2449, 2007.

[7] A. A. Arbab and G. T. Mola, "V_2O_5 thin film deposition for application in organic solar cells," *Appl. Phys*., vol. 122, p. 405, 2016.

[8] A. V. K. et al., "Preparation of anatase form of TiO_2 thin film at room temperature by electrochemical method as an alternative electron transport layer for inverted type organic solar cells," *Thin Solid Films*, vol. 706, p. 138093, 2020.

[9] C. Zhang, Yunchuan Qi [a b], Shengtang Liu [a b], Yi Men [b], Fangming Cui [a]et al., "Novel mesoporous Al-doped TiO_2 with improved lithium storage performance," *Mater. Chem. Phys*., vol. 237, p. 121822, 2019.

[10] R. Lu et al., "Visible-light-driven photoelectrochemical water oxidation with Al-doped TiO_2 nanorod arrays," *J. Alloy. Comp*., vol. 790, pp. 99-108, 2019.

[11] Y. Hu, L. Li, Z. Zhang, S. Gao, J. Guo, P. Yang, "Improving photoelectric properties by using Nb-doping on TiO_2," *Chem. Phys. Lett*., vol. 803, pp. 139830, 2022.

[12] M. N. Islam, J. Podder, "The role of Al and Co co-doping on the band gap tuning of TiO_2 thin films for applications in photovoltaic and optoelectronic devices," *Mater. Sci. in Semiconductor Processing*, vol. 121, p. 105419, 2021.

[13] Y. Liu, B. Sang, M. A. Hossain, K. Gao, H. Cheng, X. Song, S. Zhong, L. Shi, W. Shen, B. Hoex, Z. Huang, "A novel passivating electron contact for high-performance silicon solar cells by ALD Al-doped TiO_2," *Solar Energy*, vol. 228, pp. 531-539, 2021.

[14] W. A. Farooq, M. Atif, A. Fatehmulla, I. S. Yahia, M. S. AlSalhi, M. Fakhar-e-Alam, S. M. Ali, K. Ali, T. Munir, M. A. Manthrammel, "Photovoltaic and capacitance measurements of solar cells comprise of Al-doped CdS (QD) and hierarchical flower-like TiO_2 nanostructured electrode," *Renew Energy*, vol. 16, p. 102827, 2020.

[15] A. M. Xavier, I. D. Jacob, S. Surender, M. S. S. Saravana kumaar, P. Elangovan, "Structural, optical and electronic properties of copper doped TiO_2: Combined experimental and DFT study," *Inorg. Chem. Commun*., vol. 146, p. 110168, 2022.

[16] P. Londhe, N. B. Chaure, A. Athawale, "TiO_2 thin films derived by facile sol-gel method: Influence of spin rate and Al-doping on the optical and electronic properties," *Mater. Today Commun.*, vol. 29, p. 102924, 2021.

[17] K. Ancy, M. R. Bindhu, J. S. Bai, M. K. Gatasheh, A. A. Hatamleh, S. Ilavenil, "Photocatalytic degradation of organic synthetic dyes and textile dyeing waste water by Al and F co-doped TiO_2 nanoparticles," *Environ. Res.*, vol. 206, p. 112492, 2022.

[18] A. Farzaneh, M. Javidani, M. D. Esrafili, O. Mermer, "Optical and photocatalytic characteristics of Al and Cu doped TiO_2: Experimental assessments and DFT calculations," *J. Phys. Chem. Solids*, vol. 161, p. 110404, 2022.

[19] P. Joshi, S. Tiwari, K. Punia, S. Kumar, "Defect mediated mechanism in greenly synthesized undoped, Al^{+3}, Cu^{+2} and Zn^{+2} doped TiO_2 nanoparticles for tailoring bandgap, luminescence, magnetic and electrical properties," *Opt. Mater.*, vol. 132, p. 112778, 2022.

[20] M. Lal, P. Sharma, C. Ram, "Synthesis and photocatalytic potential of Nd-doped TiO_2 under UV and solar light irradiation using a sol-gel ultrasonication method," *Results in Materials*, vol. 15, p. 100308, 2022.

[21] A. Seifi, D. Salari, A. Khataee, B. Çoşut, L. Çolakerol Arslan, A. Niaei, "Enhanced photocatalytic activity of highly transparent superhydrophilic doped TiO_2 thin films for improving the self-cleaning property of solar panel covers," *Ceramics International*, vol. 49, no. 2, pp. 1678-1689, 2023.

[22] E. G. Temam, F. Djani, S. Rahmane, H. B. Temam, B. Gasmi, "Photocatalytic activity of Al/Ni doped TiO_2 films synthesized by sol-gel method: Dependence on thickness and crystal growth of photocatalysts," *Surface and Interface Analysis*, vol. 31, p. 102077, 2022.

[23] H. Y. Salah, M. Abdelfatah, A. El-Shaer, A. H. Oraby, "Effect of Al doped ZnO on optical and photovoltaic properties of the p-Cu2O/n-AZO solar cells," *Ceramics International*, vol. 49, pp. 7746-7752, 2023.

[24] P. P. Das, A. Roy, P. S. Devi, Y. Lee, "Solution processed Al-doped ZnO and its performance in dye sensitized solar cells," *Current Applied Physics*, vol. 30, pp. 69-76, 2021.

[25] W.-L. Jeong, K.-P. Kim, J.-H. Min, D.-S. Lee, "Influence of Al-doped ZnO transparent electrodes on thin-film interference in Cu2ZnSn(S,Se)4 thin-film solar cells prepared via a sputtering method," *Materials Science in Semiconductor Processing*, vol. 127, p. 105719, 2021.

[26] F. Khan, J. H. Kim, "Enhanced charge-transportation properties of low-temperature processed Al-doped ZnO and its impact on PV cell parameters of organic-inorganic perovskite solar cells," *Solid-State Electronics*, vol. 164, p. 107714, 2020.

[27] S. Park, R. Kang, S. Cho, "Effect of an Al-doped ZnO electron transport layer on the efficiency of inverted bulk heterojunction solar cells," *Current Applied Physics*, vol. 20, no. 1, pp. 172-177, 2020.

[28] F. Khan, J. H. Kim, "Enhanced charge-transportation properties of low-temperature processed Al-doped ZnO and its impact on PV cell parameters of organic-inorganic perovskite solar cells," *Solid-State Electronics*, vol. 164, p. 107714, 2020.

[29] S. M. Mustafa, A. A. Barzinjy, A. H. Hamad, S. M. Hamad, "Green synthesis of Ni doped ZnO nanoparticles using dandelion leaf extract and its solar cell applications," *Ceramics International*, vol. -, pp. 29257-29266, 2022.

[30] B. Li, N. Tang, "Study on Zr, Sn, Pb, Si and Pt doped TiO_2 photoanode for dye-sensitized solar cells: The first-principles calculations," *Chemical Physics Letters*, vol. 799, pp. 139636, 2022.

[31] C. Zhang, Y. Qi, S. Liu, Y. Men, F. Cui, "Novel mesoporous Al-doped TiO_2 with improved lithium storage performance," *Materials Chemistry and Physics*, vol. 237, p. 121822, 2019.

[32] X. Lu, X. Mou, J. Wu, D. Zhang, L. Zhang, F. Huang, F. Xu, S. Huang, "Improved-performance dye-sensitized solar cells using Nb-doped TiO_2 electrodes: efficient electron injection and transfer," *Advanced Functional Materials*, vol. 20, pp. 509-515, 2010.

[33] V. Bhosle, J. T. Prater, F. Yang, D. Burk, S. R. Forrest, J. Narayan, "Gallium-doped zinc oxide films as transparent electrodes for organic solar cell applications," Journal of Applied Physics, vol. 102, pp. 023501-023505, 2007.

[34] J. P. Kar, S. Kim, B. Shin, K. I. Park, K. J. Ahn, W. Lee, J. H. Cho, J. M. Myoung, "Influence of sputtering pressure on morphological, mechanical and electrical properties of Al-doped ZnO films," Solid-State Electronics, vol. 54, p. 1447, 2010.

[35] E. Barsoukov and J. R. Macdonald, "A Review of: 'Impedance Spectroscopy, Theory, Experiment, and Applications'," Wiley-Interscience, John Wiley & Sons, Inc., 2007.

[36] B. Conings, L. Baeten, H. Boyen, D. Spoltore, J. D'Haen, L. Grieten, P. Wagner, M. K. Van Solar Cells," Bael, J. V. Manca, "Relation between Morphology and Recombination Kinetics in Nanostructured Hybrid Solar Cells," *Journal of Physical Chemistry C*, vol. 116, no. 27, pp. 14237–14242, 2012.